Diglyme-based gel polymer electrolytes for K-ion capacitors

Binson Babu [a,b,*], Christof Neumann [b,c], Simon Muench [b,d], Marcel Enke [b,d],
Lukas Medenbach [a,b], Christian Leibing [a,b], Alexandra Lex-Balducci [b,d], Andrey Turchanin [b,c],
Ulrich S. Schubert [b,d], Andrea Balducci [a,b,*]

[a] Institute for Technical Chemistry and Environmental Chemistry, Friedrich Schiller University Jena Philosophenweg 7a, 07743 Jena, Germany
[b] Center for Energy and Environmental Chemistry Jena (CEEC Jena), Friedrich Schiller University Jena, Philosophenweg 7a, 07743 Jena, Germany
[c] Institute of Physical Chemistry, Friedrich-Schiller-University Jena, Lessingstrasse 10, 07743 Jena, Germany
[d] Laboratory of Organic and Macromolecular Chemistry (IOMC), Friedrich Schiller University Jena, Humboldtstr. 10, 07743 Jena, Germany

A B S T R A C T

In this work, we report a new diglyme-based gel-polymer electrolyte (DOKBn-GPE) suitable for the realization of a potassium-ion capacitor (KIC). We show that this novel gel polymer electrolyte displays good mechanical stability, high ionic conductivity (2.84 mS cm^{-1} at 20 °C), and broad electrochemical stability (> 5.0 V). Its use in KIC makes possible the realization of devices displaying high energy density and high stability during prolonged charge–discharge as well as during float tests. These results are indicating that the development of diglyme-based GPEs is a promising strategy for the application of high-performance K-based energy storage devices.

1. Introduction

Lithium-based energy storage technologies, such as lithium-ion batteries (LIBs), are currently the key power storage solution for electronic markets from portable to large-scale devices [1–6]. However, rising concerns over lithium resources and their uneven global distributions shifted the research to developing non-lithium-based energy storage devices [7–12]. Potassium-based systems are gaining increasing attention due to the abundance and low cost of this metal (compared to lithium) and the fact that it displays a reduction potential close to the one of lithium (−2.94 V *vs.* standard hydrogen electrode (SHE) for K$^+$/K compared to −3.04 V *vs.* SHE for Li$^+$/Li and lower than that of sodium (−2.71 V *vs.* SHE for Na$^+$/Na) [13]. Further, similar to sodium, potassium does not form an alloy with Al, making possible the utilization of the Al current collector for both the anode (negative electrode) and the cathode (positive electrode) of K-based energy storage devices [14,15]. Moreover, the K-ion-based organic electrolytes possess high ionic conductivity and good K-ion diffusion kinetics. These favourable features are possible due to the weaker Lewis acidity of K$^+$ and the low desolvation energy, which are leading to smaller Stokes' radius/solvated ions (3.6Å) compared to that of Li-ion (4.8Å) and Na-ion (4.6Å) [16–19].

In the last years, several studies have been dedicated to the development of electrode materials and electrolytes suitable for K-based devices as well as to the electrode/electrolyte interfaces of these systems [14,19,20]. Currently, liquid electrolytes based on the mixtures of potassium salts and organic solvents can be considered state-of-the-art electrolytes for K-based energy storage devices such as K-ion batteries (KIBs) and K-ion capacitors (KICs) [20–24]. However, like in any electrochemical energy storage device, the use of liquid electrolytes limits the overall safety of the devices due to the high volatility and flammability of the electrolyte components and the possibility of electrolyte leakage. For this reason, several alternative electrolytes have been considered in the last few years [25,26]. Among them, those based on gel-polymer electrolytes (GPEs), in which a liquid electrolyte (LE) is immobilized into a polymer matrix, are considered very promising [27, 28]. GPEs display good ionic conductivity (~10^{-3} S cm^{-1}) at room temperature and good mechanical stability [29–32]. Hence, their use can improve safety and, also, can allow the realization of flexible energy storage devices. So far, only a rather limited number of K-based GPEs have been reported. Most of these studies considered GPEs based on polymer matrixes such as polyacrylonitrile (PAN) [33,34], poly(vinylidene fluoride-*co*-hexafluoropropylene) (PVdF–HFP) [35], poly(methyl methacrylate) (PMMA) [30] used in combination with ester (carbonate) based solvents. Recent works showed that the use of ether-based

* Corresponding authors at: Institute for Technical Chemistry and Environmental Chemistry, Friedrich Schiller University Jena Philosophenweg 7a, 07743 Jena, Germany.

E-mail addresses: binson.babu@uclouvain.be (B. Babu), andrea.balducci@uni-jena.de (A. Balducci).

electrolytes is particularly promising for the realization of high-performance K-based devices [19,35–39]. For this reason, these electrolytes are currently considered among the most interesting for the development of advanced K-based systems. To the best of our knowledge, however, the development and use of diglyme-based GPEs have not been considered to date.

In this study, we present a new gel-polymer electrolyte containing a methacrylate-based polymer matrix and a diglyme-based liquid electrolyte (DOKBn-GPE) suitable for K-based energy storage devices. Initially, the conductivity, thermal and electrochemical stability of the new DOKBn-GPE are investigated and compared with those of the "neat" liquid electrolyte (1 M KPF$_6$ in diglyme). Afterward, the use of the novel DOKBn-GPE on KIC containing Prussian white (PW) and activated carbon (AC) based electrodes is considered. The electrochemical performance of these devices and their aging processes are investigated in detail and are compared with those of systems containing the liquid electrolyte.

2. Experimental section

2.1. Preparation and characterization of DOKBn-GPE

The matrix polymerization process has been reported in our previous publications [28,40,41]. In short, the polymer was prepared by mixing 1 mmol oligo (ethylene glycol) methyl ether methacrylate (OEGMA) and 3 mmol benzyl methacrylate (BnMA) with 0.2 wt% benzophenone and placing the resulting mixture between two siliconized PET foils for polymerization for 1 hour by UV-irradiation. To remove the inhibitors, the monomers were passed over a short column of inhibitor remover. Afterward, disks of the polymer film were punched out and dried overnight at 120 °C under a vacuum. Subsequently, the gel polymer electrolyte (DOKBn-GPE) was prepared by soaking the polymer films with 1 M KPF$_6$ in diglyme (polymer: LE = 1:5) overnight under an inert atmosphere. All the chemicals utilized in the above processes are commercially purchased from Merck.

2.2. Characterization of DOKBn-GPE and liquid electrolyte

The temperature-dependent conductivity measurements were conducted in a climatic chamber (Binder -Alternating Climate Chamber MK056) with the DOKBn-GPE placed in a closed cell (TSC Battery cell from rhd instruments) between two stainless steel electrodes, and the liquid electrolyte (LE) was placed in sealed cells with Pt-plated electrodes. All the ionic conductivities were calculated through impedance measurements carried out using ModuLabXM (Solartron analytical) potentiostat in a frequency range comprise between 300 kHz to 1 Hz, with an amplitude of 5 mV and within a temperature range from 0 to 60 °C.

The thermogravimetric analysis (TGA) measurements were carried out using a Netzsch TG 209 F1 Libra under a nitrogen atmosphere with a heating rate of 20 K min^{-1}.

The electrochemical stability window (ESW) of the DOKBn-GPE and LE was investigated utilizing linear sweep voltammetry (LSV). During the test, stainless steel (area 1.13 cm^2, diameter 12 mm) was used as the working electrode (WE), and an oversized AC electrode was used as the counter electrode. Metallic potassium was used as the reference electrode. All the measurements were conducted in a three-electrode configuration (Swagelok®-type cell). For the investigation of the GPE, the DOKBn-GPE was placed between the WE and CE. In the case of the LE, a Whatman GF/D glass microfiber filter (675 μm thickness and 13 mm diameter) soaked with 150 μL of 1 M KPF$_6$ in diglyme electrolyte was used as the separator. Independently of the used electrolyte, a scan rate of 0.5 mV s^{-1} was applied to investigate the anodic and cathodic limits [28].

2.3. Electrode preparation and device fabrication

Prussian white (PW) electrodes were prepared by utilizing 70 wt% of self-made K$_2$Fe[Fe(CN)$_6$] (synthesized through a room-temperature precipitation method reported in reference) [22], 20 wt% C—NERGY Super C65 (*Imerys*) and 10 wt% polyvinylidene fluoride (*Sigma Aldrich*) as the conducting agent and binder, respectively. N-Methyl-2--pyrrolidone (NMP, *Sigma Aldrich*) was utilized in the above mixture to make a slurry that was coated on an aluminum foil in an argon-filled glovebox (*MBraun*, H$_2$O and O$_2$ < 1 ppm) [28,40]. The electrodes were kept at 100 °C for at least 12 h under a vacuum for drying. The punched PW electrodes had an area of 1.13 cm^2 and an active mass loading of 2.0–4.5 mg cm^{-2}.

Activated carbon (AC) electrodes were prepared by utilizing 85 wt% Super 30-DLC Super (*Norit*) as the active material, 10 wt% C—NERGY Super C65 (*Imerys*), and 5 wt% polyvinylidene fluoride (*Sigma Aldrich*) as the conducting agent and binder, respectively [42]. In this case, the mixtures were dissolved in ethanol solution and stirred at 90 °C until a thick solid slurry formed. The latter was flattened to make a uniform free-standing film having an area of 1.13 cm^2. Electrodes with two different active mass loadings were prepared. In the case of the investigation of the KIC, an electrode with active mass loading of 2.0–4.5 mg cm^{-2} was used. During the investigation of the PW-based electrodes, oversized electrodes with a mass loading of ∼ 50 mg cm^{-2} were utilized.

All the investigated cells were fabricated using a Swagelok®-type cell, assembled under an argon-filled glove box. For the half-cell characterization of PW (in both electrolytes) a three-electrode configuration with PW electrodes as working electrode (WE), oversized AC as the counter electrode (CE), and K-metal as reference electrode (RE) was used. In the case of systems containing the LE, a Whatman GF/D glass microfiber filter (675 μm thickness and 13 mm diameter) drenched with 150 μL of 1 M KPF$_6$ in diglyme electrolyte was used as the separator. In the case of GPEs, the DOKBn-GPE was introduced between the electrodes.

The KIC investigated in this work featured an active mass ratio equal to 1:1 between positive PW electrodes and negative AC film electrodes. All the tests have been carried out in 3 electrode configurations.

2.4. Electrochemical characterization of devices

All the electrochemical characterizations were conducted with a multichannel electrochemical workstation (VMP3, Biologic), MPG-2 (*BioLogic*), or LBT21084 (*Arbin Instruments*)) battery cycler at room temperature.

Galvanostatic charge-discharge (GCD) measurements were conducted in a potential window of 2.8–4.2 V *vs.* K$^+$/K for the half-cell characterization of PW electrodes, and for KICs, the device was cycled in a voltage window of 0.0 to 3.0 V. Further, the aging of KICs was tested by a sequence of electrochemical experiments identical to that utilized by our group for the investigation of lithium-ion capacitors [40]. The initial aging test analysis is conducted after cycling the device for a long time in a voltage window of 0.0 to 3.0 V at a current density of 0.25 A g^{-1}. For the float test analysis, the KICs were initially activated by carrying out 10 GCD cycles between 0.0 and 3.0 V at a current density of 0.25 A g^{-1}. Afterward, the devices were charged to 3.0 V at a current density of 0.25 A g^{-1} and were held at this voltage for 20 h. This float test protocol mentioned above was repeated 10 times.

The energy and power density of KICs were evaluated by using the following equations [43–46]:

$$\text{Specific power density, } P_s = \frac{V \times I}{M} \tag{1}$$

$$\text{Specific energy density, } E_s = P_s \times t \tag{2}$$

where, $V = \frac{V_{max} + V_{min}}{2}$, V_{max} and V_{min} are the maximum and minimum

voltage of the galvanostatic discharge curve of the KIC after excluding the ohmic drop, *I* is the current applied, *M* is the total active mass of both electrodes (~ 5 mg for AC//PW) and *t* is the time taken for discharging.

2.5. Postmortem analysis

After the electrochemical tests, the KICs were disassembled and a postmortem analysis of the electrodes (both positive and negative) have been carried out employing XPS, SEM, and EDX. All the electrodes subjected to postmortem studies were not washed to preserve every compound formed at the surface. The electrodes from LE-based KICs were mounted on the sample holders mechanically whereas conductive carbon tape was used for fixing the electrodes from GPE-based KICs due to the high sticking. To avoid direct air contact with the electrodes, all these processes were carried out inside the glove box in Ar-atmosphere. Subsequently, all the samples were transferred to a gas-tight box filled with Ar for the postmortem analysis. Initially, the samples were introduced into the ultra-high vacuum for XPS analysis followed by Scanning electron microscope (SEM) and Energy dispersive X-Ray (EDX)

measurements in a high vacuum chamber using a similar sample transfer method.

The XPS was operated in a UHV Multiprobe system (*Scienta Omicron*) using a monochromatic X-ray source (Al K$_\alpha$) and an electron analyzer (Argus CU) with a spectral resolution of 0.6 eV. All the XPS measurements were carried out at a very low pressure of < 2 × 10^{-10} mbar. An electron flood gun (NEK150SC, Staib, Germany) at 6 eV and 50 µA were used for charge compensation during data acquisition in each sample. All the spectra obtained were fitted using Voigt functions after background subtraction and the C1s peak (284.3 eV) was utilized for calibrating the bare PW and AC electrodes. The depth profile with an approximate sputter depth of 2 to 5 nm was taken by sputtering the samples with Ar$^+$ ions (FOCUS FDG150, 1 keV, 10 mA) for 10 min. Here, in addition to the spectra calibrated using the C 1 s peak, each high-resolution spectra might be broadened or shift by 1–2 eV in binding energy due to the known effect in XPS analysis of battery electrodes [47]. However, despite this, it is possible to identify the different species in the spectra reliably. Further, the morphological and elemental mapping of the electrodes were taken by utilizing SEM and EDX (*Zeiss Sigma*
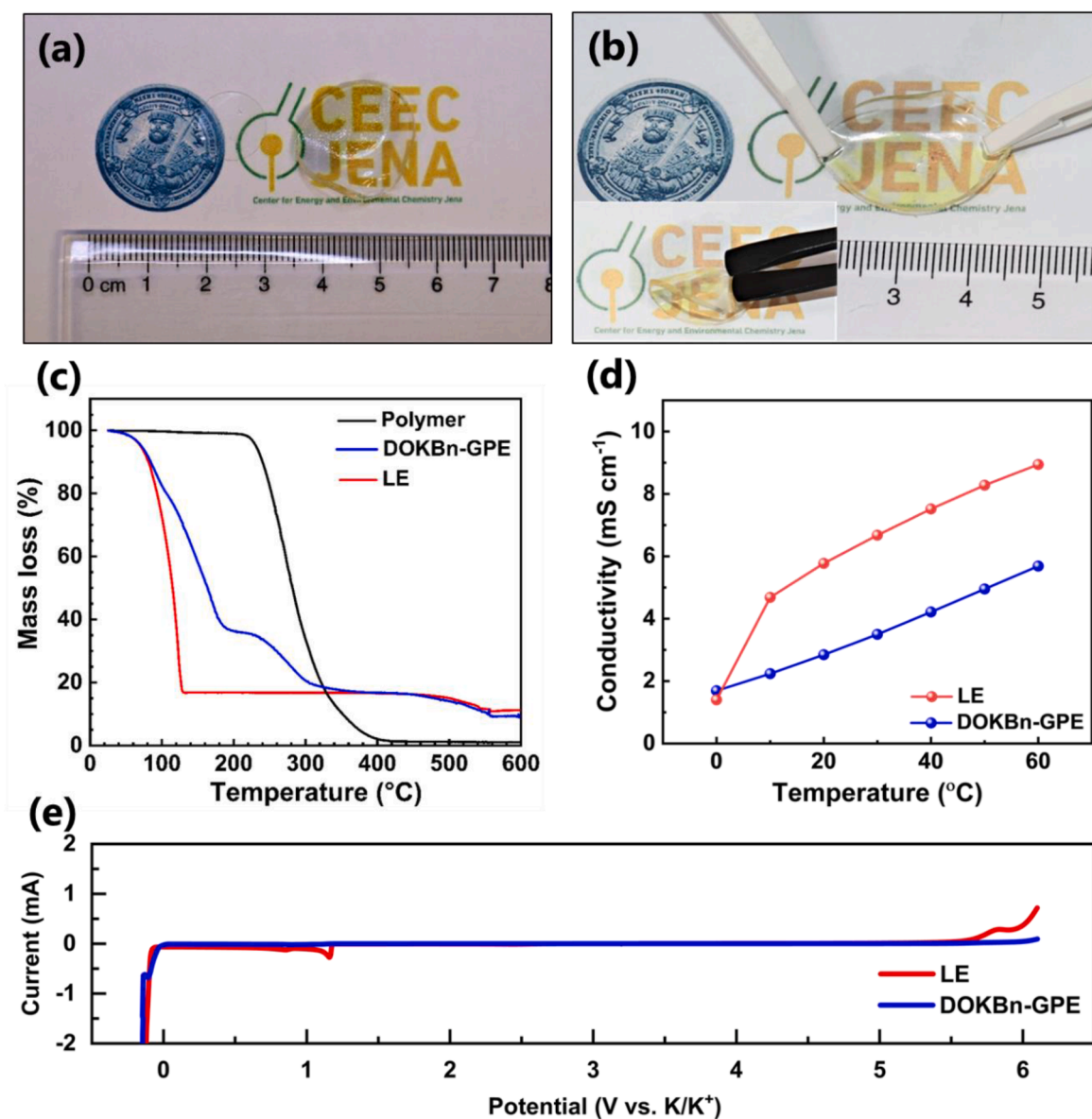

Fig. 1. (a) Photograph of the polymer film and the gellated DOKBn-GPE, (b) mechanical properties of the DOKBn-GPE, (c) comparison of the thermal stability of LE, polymer, and DOKBn-GPE, (d) temperature dependence of the ionic conductivity of DOKBn-GPE and LE, (e) comparison of ESW of the DOKBn-GPE and LE determined by linear-sweep voltammetry (scan rate of 0.5 mV s^{-1}).

VP) with a beam energy of 15 kV using the secondary electron detector of the system. An Oxford system and a 50 mm^2 XMax detector with a resolution of 127 eV were used for EDX analysis.

3. Results and discussion

3.1. Synthesis and characterization of diglyme-based gel GPEs

The polymer matrix used for the realization of the GPE investigated in this work was synthesized by the polymerization of OEGMA and BnMA with benzophenone in presence of UV-light irradiation (see Experimental section). The polymerization kinetics and the mechanical properties of the polymer matrix have been already discussed in our previous work, and they will not be considered again in the present study [28,40,41]. A free-standing GPE was obtained by gelating the polymer matrix with the liquid electrolyte 1 M KPF$_6$ in Diglyme for 12 h. After this time, the liquid uptake was 420%, which is slightly higher compared to other types of liquid electrolytes in the same polymer matrix (see Table S1 of SI). In the following, the GPE considered in this work will be referred to as DOKBn-GPE. Fig. 1a and b illustrates the high mechanical stability of DOKBn-GPE and its suitability to be used as a separator for electrochemical devices. Fig. 1c is showing a comparison of the thermal stability of DOKBn-GPE, the liquid electrolyte (indicates as LE), and the polymer matrix. As shown, the temperature (T_d) of DOKBn-GPE and LE at which weight loss started is comparable (*ca.* 46 °C), and is much lower than that of the polymer matrix (~ 210 °C).

The difference is caused by the evaporation of the volatile diglyme solvent due to its high vapor pressure. Nonetheless, it has to be mentioned that the presence of the polymeric matrix is reducing the kinetics of evaporation of the LE. Fig. 1d compares the ionic conductivities (σ) of DOKBn-GPE and LE in the temperature range comprising from 0 to 60 °C. At 20 °C, the LE displays an ionic conductivity of 5.80 mS cm^{-1}, while the conductivity of DOKBn-GPE is 2.84 mS cm^{-1}. This latter value is certainly promising for a GPE, and it is comparable to that of several K-based GPEs investigated so far (Table S2 in SI). As expected, the ionic conductivity of both electrolytes increases with rising temperature. Fig. 1e shows the electrochemical stability window (ESW) of the investigated electrolytes. As visible, both electrolytes display overall stability exceeding 5 V (from 0 V *vs.* K$^+$/K to more than 5.0 V *vs.* K$^+$/K). Taking these results into account, DOKBn-GPE appears to display a set of properties that make it suitable for application in K-based energy storage devices. In the following, the use of DOKBn-GPE in KICs will be considered, and, through the manuscript, the results obtained with this innovative GPE will be compared with those obtained with the LE.

3.2. DOKBn-GPE-based K-ion capacitor

KICs (as any other metal-ion capacitor) can be realized utilizing different combinations of battery and supercapacitor electrodes. In the case of this work, we decided to realize KICs containing a positive electrode having PW as the active material and an AC-based negative electrode. The advantage of this combination (which is sometimes
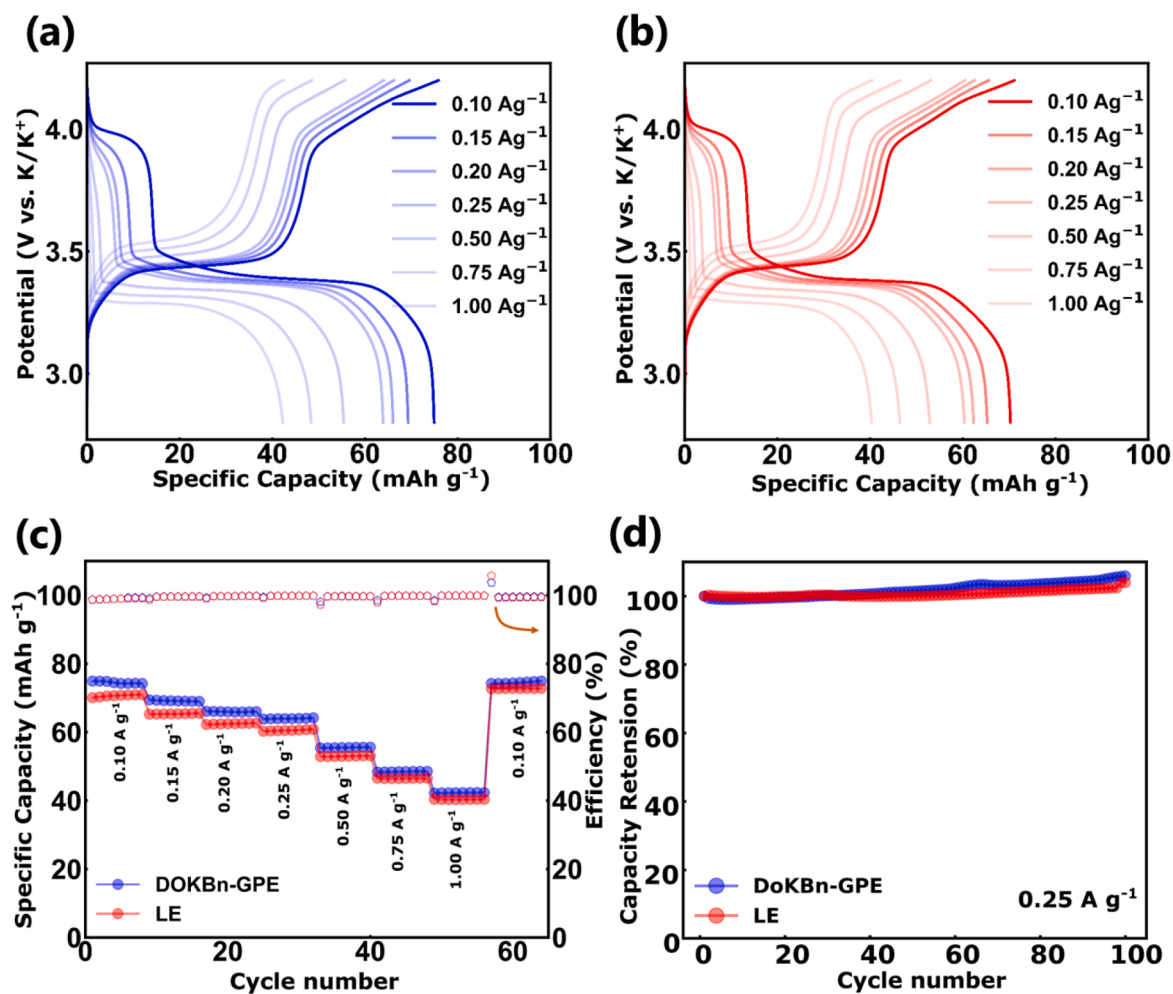

Fig. 2. Electrochemical characterization of Prussian white (PW) electrodes: Voltage profile of PW electrodes in (a) DOKBn-GPE and (b) LE obtained at different current densities in a potential window of 2.8–4.2 V *vs.* K$^+$/K, (c) rate performance of the electrodes, and (d) cycling stability (based on the discharge capacity) during charge-discharge performed at a current density of 0.25 A g^{-1}.

indicated as a Type 2 configuration) [12] is related to the presence of an inner source of potassium ions, in this case, the PW, within the device. During the charge/discharge process of this KIC, the K-ions undergo a de-insertion/insertion at the positive electrode, whereas at the negative electrode a simultaneous adsorption/desorption of K-ions takes place.

Initially, the behavior of the PW electrode in combination with DOKBn-GPE and LE was investigated. For this investigation, an oversize AC-based electrode was used (all the detail about the cell assembly and measurements are reported in the experimental part) and charge-discharge has been carried out at the potential comprising between 2.8 and 4.2 V *vs.* K$^+$/K. Fig. 2a shows the voltage profiles at different current densities of the PW electrode when used in combination with the DOKBn-GPE. Those of the electrodes cycled in combination with LE are shown in Fig. 2b. As visible, at low current density (0.1 A g^{-1}), the PW electrodes display two voltage plateaus, corresponding to the redox

processes responsible for the phase change from Prussian white (PW) to Prussian blue (PB) (3.4 V *vs.* K$^+$/K) and to Prussian green (PG) (4.0 V *vs.* K$^+$/K), which are visible in both electrolytes [22]. These plateaus are well visible even at a high current density (1.0 A g^{-1}). The occurrence of these reactions can also be observed while considering the changes in differential capacity (see Fig. S1 in the supplementary information (SI)). It is interesting to notice that the coulombic efficiency, specific capacity, and capacity retention of the PW electrode are very comparable in DOKBn-GPE and LE. At 0.1 A g^{-1}, the PW electrode used in combination with DOKBn-GPE exhibits a discharge capacity of 75 mAh g^{-1}, while that cycled in LE of 71 mAh g^{-1}. In both electrolytes, the coulombic efficiency during the charge–discharge process was higher than 99% (Fig. 2c). The PW electrodes display also the same capacity retention in the two investigated electrolytes. For example, when a current density of 1.0 A g^{-1} was applied, the electrode displayed a discharge capacity of 40
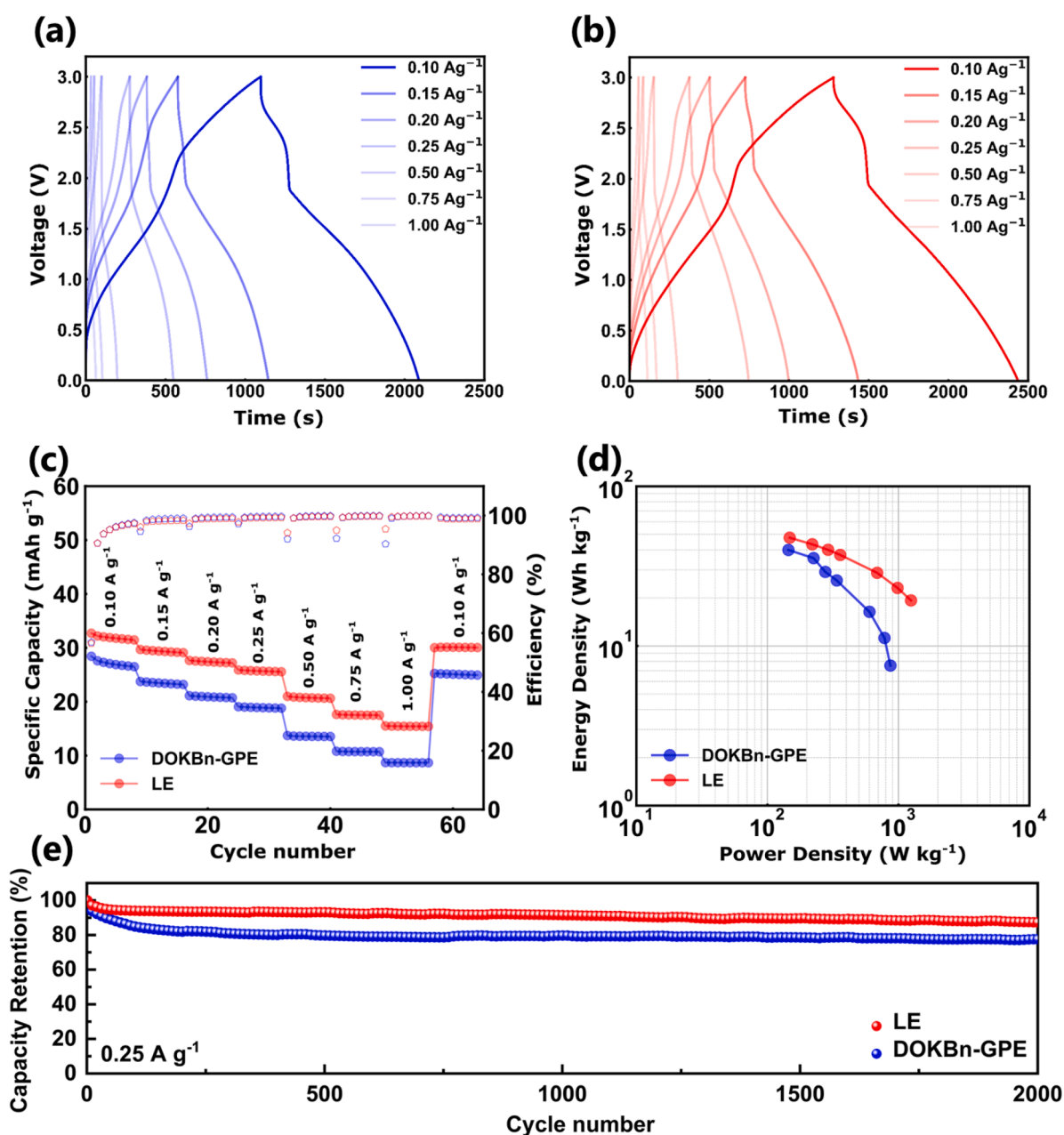

Fig. 3. Electrochemical performance of KICs containing DOKBn-GPE (*p*-KIC) and LE (*l*-KIC) as electrolytes: charge/discharge profiles of (a) *p*-KIC and (b) *l*-KIC at different current densities, (c) capacity retention at different current densities, (d) Ragone plot and (e) stability during charge–discharge measurements carried out at 0.25A g^{-1} (based on the total active mass of both electrodes) in a voltage window of 0.0 to 3.0 V.

mAh g^{-1} in DOKBn-GPE and LE. Further, it is worth noticing that the use of DOKBn-GPE is not adversely affecting the electrode stability. As shown in Fig. 2d (and in Fig. S2a and S2b of SI), during 100 charge–discharge cycles carried out at 0.25 A g^{-1} the PW was able to retain all its initial capacity, independently of the used electrolyte. It has to be also remarked that the electrochemical behavior observed for the PW electrode cycled in the DOKBn-GPE is better than that reported for many cathode materials for the K-based system (see Table S3 in SI). Taking these results into account, it is evident that the new DOKBn-GPE investigated in this work is highly compatible with the PW electrodes and can be utilized for the realization of KICs.

Afterward, taking into account the results discussed above, a lab-scale KIC containing a PW-based positive electrode, an AC-based negative electrode (having a mass ratio of 1:1), and DOKBn-GPE as an electrolyte were realized and tested. To compare the performance of this innovative KIC with that of a device containing liquid electrolyte, also a KIC containing the same electrodes but the LE was considered. In the following, the devices will be indicated as *p*-KIC and *L*-KIC, respectively. Both of them have been tested between 0 and 3 V. This mass ratio and operative voltage have been selected as they were the one allowing the best cycling stability. Figs. 3a and b show the charge-discharge curve of *p*-KIC and *L*-KIC, respectively, at current densities ranging from 0.1 A g^{-1} to 1.0 A g^{-1}. As shown, both devices display similar charge–discharge profiles and comparable coulombic efficiencies (>99%). However, the specific capacity (based on the mass of both electrodes) of *p*-KIC is slightly lower than that of *L*-KIC, *e.g.* at 0.10 A g^{-1} the former displays 27 mAh g^{-1} while the latter is 32 mAh g^{-1}. This difference in capacity can be ascribed to the higher resistance displayed by the DOKBn-GPE, which is affecting the behavior of the AC-based electrode (Fig. S3 in SI). Nevertheless, it is noteworthy to observe that both KICs demonstrate comparable capacity retention throughout the considered current densities (Fig. 3c). Fig. 3d compares the energy and power densities of the two KICs in a Ragone plot. As shown, both KIC display promising energy values (40 Wh kg^{-1} and 48 Wh kg^{-1} at 0.1 A^{-1} for *p*-KIC and *L*-KIC, respectively) and good power densities, although the one of *p*-KIC is slightly lower than that of *L*-KIC (868 W kg^{-1} and 1247 W kg^{-1} at 1.0 Ag^{-1} for *p*-KIC and *L*-KIC, respectively) for the reason discussed above. As shown in Fig. 3e and Fig. S4, the two KICs display very good cycling stability. After 2000 cycles carried out at a current density of 0.25 A g^{-1} *L*-KIC displays capacity retention of 87%. On the other hand, *p*-KIC loses 20% of the initial capacity within the initial 300 cycles and then attains an almost steady value securing 78% at the end of the cycling process.

The performance of *p*-KIC indicates that the new DOKBn-GPE is a suitable electrolyte for the realization of high-performance KICs. Certainly, further optimization is needed to improve the performance of this device, and especially its power. Nonetheless, it is important to notice that the electrochemical performances exhibited by *p*-KIC are already comparable for this kind of K-based device (see Table S4 of SI). Moreover, it is also interesting to notice that the investigated KICs are showing higher performance than AC- based symmetric supercapacitor
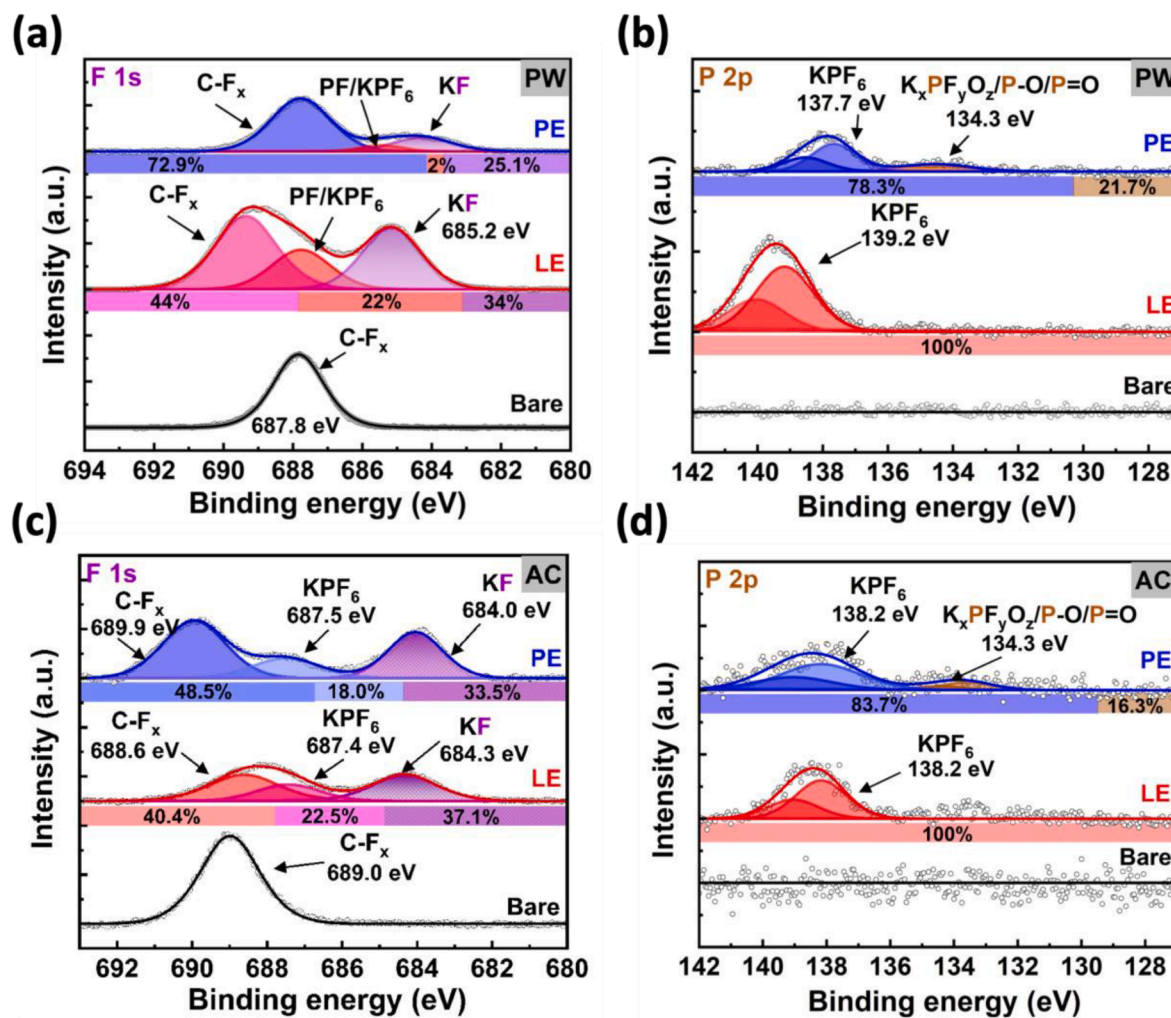

Fig. 4. postmortem XPS measurement of the (a) and (b) PW, and (c) and (d) AC of *p*-KIC and *L*-KIC after 2000 charge-discharge cycles at 0.25A g^{-1} in a voltage window of 0.0 to 3.0 V.

containing the same electrolytes (see Fig. S5 and S6 in SI). Further, the *p*-KIC shows better cycling stability than the previously reported Na-ion capacitor with the same polymer matrix in NaPF$_6$ liquid electrolyte [28].

To understand the influence of both electrolytes on the aging of KICs at the end of the cycling process, several postmortem analyses were carried out on the electrodes of the investigated devices. From the SEM images, the morphology of the electrodes did not result significantly altered by the cycling process (see Figs. S8 and S9 of SI). On the other hand, after cycling, an increase in fluorine and phosphorous content was visible in both electrodes (Figs. S5 and S6 of SI). XPS was used to elucidate the chemical compositions at the electrode/electrolyte interfaces on both positive and negative electrodes (Fig. 4 and Fig. S10 of SI). The large peaks observed in both electrodes, before and after cycling, for the de-convoluted high-resolution F 1s spectra (around 689–688 eV) represent the CF species originating from the PVDF binder [48]. An increase in the concentration of KF species (684–685 eV) was observed in the F1s of both KICs after cycling, indicating the decomposition of the potassium salt (KPF$_6$ → KF + PF$_5$) or its hydrolysis (KPF$_6$ + H$_2$O$_{(trace)}$ → KF + 2HF + OPF$_3$) in presence of trace amount of water [48,49]. On the other hand, while considering the high-resolution P 2p spectra (Figs. 4b and d), the presence of phosphorous compounds (K$_x$PF$_y$O$_z$/P—O/P=O) was only prominent in the electrodes that were used in combination with DOKBn-GPEs, indicating the occurrence of additional decomposition processes in this electrolyte (compared to the liquid), which might be the reason for the comparatively large decline in the *p*-KIC capacity during cycling (Fig. 3e).

To further investigate the stability and the aging processes occurring in the investigated KICs, a series of float tests were conducted (the details about the utilized protocol are reported in the experimental part). Float tests are used to investigate the stability of electrochemical double layer capacitors and, as shown in recent work, they are also very useful to understand the aging processes taking place in metal-ion capacitors [40]. Fig. 5 compares the evolution of the capacity of *p*-KIC and *L*-KIC during the float test carried out at 3.0 V for a total of 200 h. As shown, both devices display a rather comparable behavior during the time of floating time (see Fig. S11 in SI). At the beginning of the floating process (first 20 h), both KICs show a loss of initial capacity (15% for *p*-KIC and 11% for *L*-KIC). Afterward, the capacity of both devices increases again and after 80 h of floating, *p*-KIC and *L*-KIC are displaying 93% and 100% of their initial capacity, respectively. This behavior might be caused by

changes in the electrode/electrolyte interface and/or by an improved electrode wetting, which results in an improvement in the capacity. Subsequently, *p*-KIC displayed a gradual decrease in capacity, and after 200 h of floating was able to retain 77% of its initial capacity. On the other hand, *L*-KIC display better stability, and after 200 h of floating the device was able to retain 97% of its initial capacity. The different stability of the two devices can be caused by different factors. One of them can be the different drifts experienced by their electrodes during the float test. As shown in Fig. S11c and S11d of SI, the electrodes of *p*-KIC are shifting from their initial voltage region towards an unstable region much more than those of the *L*-KIC.

To gain a better understanding of the aging of both KICs during the floating test, a postmortem analysis of the electrodes in the investigated KICs was carried out. As in the case of the cycling process, the SEM images reveal that the morphology of PW and AC electrodes does not change significantly at the end of the test. Also, the EDX elemental analysis shows an increase in fluorine and phosphorous content, as the one observed during the cycling process (see Figs. S12 and S13 in SI). XPS analysis shows the occurrence of a change in concentration of KF and K$_x$PF$_y$O$_z$/P—O/P=O species in both electrodes and electrolytes (Fig. 6). It has to be mentioned that the presence of K$_x$PF$_y$O$_z$/P—O/P=O in both electrodes after the floating test is higher compared to the one observed during the cycling, particularly in the case of the electrodes from *l*-KIC. In the case of electrodes from *p*-KIC, the presence of K$_x$PF$_y$O$_z$/P—O/P=O in both electrodes is visible after both cycling and floating.

Considering these results, the degradation processes taking place in the investigated devices appears mainly caused by the formation of fluorinated compounds which are precipitating on the electrode surface. The nature of these compounds, however, does not seems to be much affected by the polymeric matrix of the gel-polymer electrolyte. In the future, it will be important to gain more information about the impact of the solvent of the degradation processes taking place on the investigated KIC.

4. Conclusion

In this study, we reported for the first time about a diglyme-based gel polymer electrolyte (DOKBn-GPE) suitable for K-based storage devices. We showed that this innovative methacrylate-based gel polymer electrolyte displays good mechanical stability, high ionic conductivity (2.84 mS cm^{-1} at 20 °C), and broad electrochemical stability (> 5.0 V) and can be successfully introduced in KICs. We demonstrated that KICs containing DOKBn-GPE (*p*-KIC) display high energy density (40 Wh kg^{-1} at 0.10 A g^{-1}) and high stability during prolonged charge-discharge (capacity retention of 78% after 2000 cycles) as well as during float test (capacity retention of 77% after 200 h of float at 3 V). This performance is comparable to that observed in a device containing the same electrode but the "neat" liquid electrolyte (*l*-KIC).

These results indicate that the use of diglyme-based GPEs is a promising strategy for the realization of high-performance K-based energy storage devices.

Credit author statement

Binson Babu, Christof Neumann, Simon Muench, Marcel Enke, Lukas Medenbach and Christian Leibing carried out the experimental work reported in the manuscript and wrote the article draft.

Alexandra Lex-Balducci, Andrey Turchanin, Ulrich S. Schubert and Andrea Balducci wrote/finalized the article and supervised the work of Binson Babu, Christof Neumann, Simon Muench, Marcel Enke, Lukas Medenbach and Christian Leibing

Declaration of Competing Interest
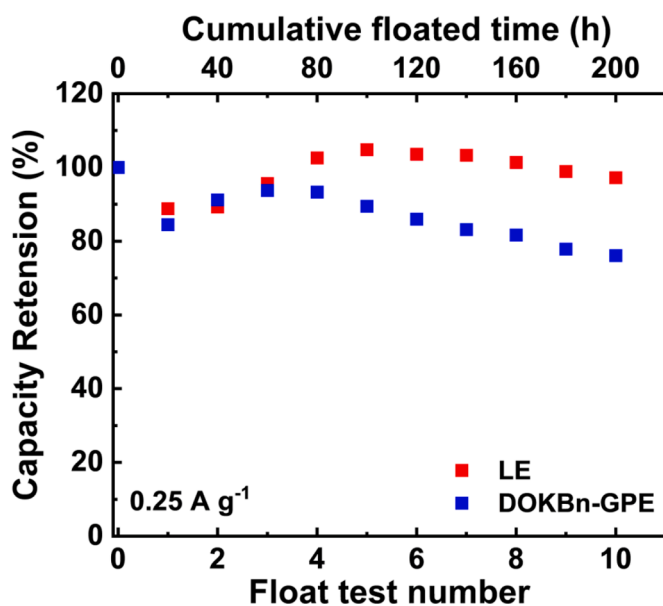
The authors declare that there is no conflict of interests.

Fig. 5. Capacity retention of *p*-KIC and *L*-KIC during the float test carried out at 3.0 V.
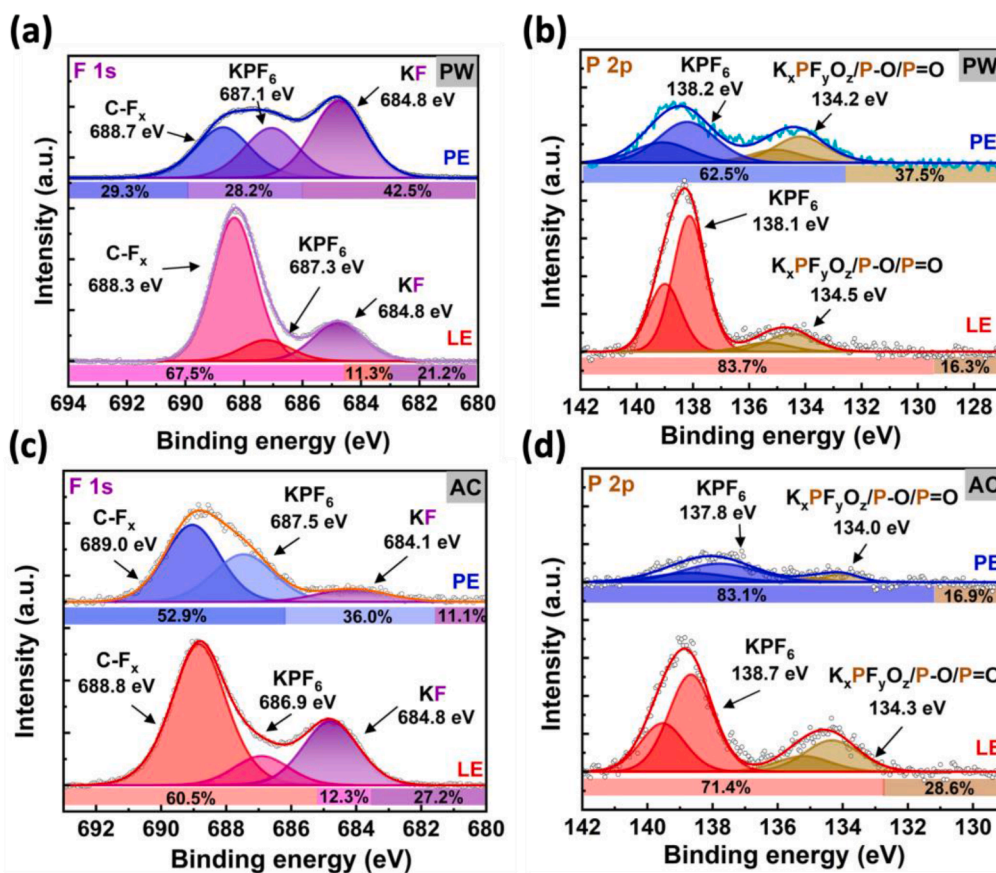
Fig. 6. Postmortem XPS measurement of (a) and (b) PW, and (c) and (d) AC of *p*-KIC and *L*-KIC after 200 h of floating at 3.0 V.

Data availability

Data will be made available on request.

Supplementary materials

Supplementary material associated with this article can be found, in the online version, at doi:10.1016/j.ensm.2023.01.031.

References

[1] T. Kim, W. Song, D.-.Y. Son, L.K. Ono, Y. Qi, Lithium-ion batteries: outlook on present, future, and hybridized technologies, J. Mater. Chem. A 7 (2019) 2942–2964, https://doi.org/10.1039/C8TA10513H.

[2] S. Pal, X. Zhang, B. Babu, X. Lin, J. Wang, A. Vlad, Materials, electrodes, and electrolytes advances for next generation lithium-based anode-free batteries, Ox. Open Mater. Sci. (2022), https://doi.org/10.1093/oxfmat/itac005 itac005.

[3] W.-J. Kwak, D.S. Rosy, C. Xia, H. Kim, L.R. Johnson, P.G. Bruce, L.F. Nazar, Y.-. K. Sun, A.A. Frimer, M. Noked, S.A. Freunberger, D. Aurbach, Lithium-oxygen batteries and related systems: potential, status, and future, Chem. Rev. 120 (2020) 6626–6683, https://doi.org/10.1021/acs.chemrev.9b00609.

[4] X.-.B. Cheng, R. Zhang, C.-.Z. Zhao, Q. Zhang, Toward safe lithium metal anode in rechargeable batteries: a review, Chem. Rev. 117 (2017) 10403–10473.

[5] J.B. Robinson, K. Xi, R.V. Kumar, A.C. Ferrari, H. Au, M.-.M. Titirici, A. Parra-Puerto, A. Kucernak, S.D.S. Fitch, N. Garcia-Araez, Z.L. Brown, M. Pasta, L. Furness, A.J. Kibler, D.A. Walsh, L.R. Johnson, C. Holc, G.N. Newton, N. R. Champness, F. Markoulidis, C. Crean, R.C.T. Slade, E.I. Andritsos, Q. Cai, S. Babar, T. Zhang, C. Lekakou, N. Kulkarni, A.J.E. Rettie, R. Jervis, M. Cornish, M. Marinescu, G. Offer, Z. Li, L. Bird, C.P. Grey, M. Chhowalla, D.D. Lecce, R. E. Owen, T.S. Miller, D.J.L. Brett, S. Liatard, D. Ainsworth, P.R. Shearing, 2021 roadmap on lithium sulfur batteries, J. Phys. Energy 3 (2021) 031501, https://doi.org/10.1088/2515-7655/abdb9a.

[6] C.P. Grey, D.S. Hall, Prospects for lithium-ion batteries and beyond-a 2030 vision, Nat. Commun. 11 (2020) 6279, https://doi.org/10.1038/s41467-020-19991-4.

[7] A. Ponrouch, J. Bitenc, R. Dominko, N. Lindahl, P. Johansson, M.R. Palacin, Multivalent rechargeable batteries, Energy Storage Mater. 20 (2019) 253–262, https://doi.org/10.1016/j.ensm.2019.04.012.

[8] J. Wang, A. Vlad, Empowering magnesium, Nat. Energy 5 (2020) 945–946, https://doi.org/10.1038/s41560-020-00744-y.

[9] Y. Tian, G. Zeng, A. Rutt, T. Shi, H. Kim, J. Wang, J. Koettgen, Y. Sun, B. Ouyang, T. Chen, Z. Lun, Z. Rong, K. Persson, G. Ceder, Promises and challenges of next-generation "Beyond Li-ion" batteries for electric vehicles and grid decarbonization, Chem. Rev. 121 (2021) 1623–1669, https://doi.org/10.1021/acs.chemrev.0c00767.

[10] E. Fan, L. Li, Z. Wang, J. Lin, Y. Huang, Y. Yao, R. Chen, F. Wu, Sustainable recycling technology for Li-ion batteries and beyond: challenges and future prospects, Chem. Rev. 120 (2020) 7020–7063, https://doi.org/10.1021/acs.chemrev.9b00535.

[11] K. Kubota, M. Dahbi, T. Hosaka, S. Kumakura, S. Komaba, Towards K-ion and Na-ion batteries as "beyond Li-ion, Chem. Rec. 18 (2018) 459–479, https://doi.org/10.1002/tcr.201700057.

[12] B. Babu, P. Simon, A. Balducci, Fast charging materials for high power applications, Adv. Energy Mater. 10 (2020), https://doi.org/10.1002/aenm.202001128, 2001128.

[13] A.V.B. John, M. Td, Potassium-ion batteries: key to future large-scale energy storage? ACS Appl. Energy Mater. 3 (2020) 9478–9492, https://doi.org/10.1021/acsaem.0c01574.

[14] J.-.Y. Hwang, S.-.T. Myung, Y.-.K. Sun, Recent progress in rechargeable potassium batteries, Adv. Funct. Mater. 28 (2018), 1802938, https://doi.org/10.1002/adfm.201802938.

[15] J. Chen, D.H.C. Chua, P.S. Lee, The advances of metal sulfides and in situ characterization methods beyond Li ion batteries: sodium, potassium, and

aluminum ion batteries, Small Methods 4 (2020), 1900648, https://doi.org/10.1002/smtd.201900648.

[16] T. Hosaka, K. Kubota, A.S. Hameed, S. Komaba, Research development on K-ion batteries, Chem. Rev. 120 (2020) 6358–6466, https://doi.org/10.1021/acs.chemrev.9b00463.

[17] J. Li, Y. Hu, H. Xie, J. Peng, L. Fan, J. Zhou, B. Lu, Weak cation–solvent interactions in ether-based electrolytes stabilizing potassium-ion batteries, Angew. Chem. Int. Ed. 61 (2022), e202208291, https://doi.org/10.1002/anie.202208291.

[18] M. Okoshi, Y. Yamada, S. Komaba, A. Yamada, H. Nakai, Theoretical analysis of interactions between potassium ions and organic electrolyte solvents: a comparison with lithium, sodium, and magnesium ions, J. Electrochem. Soc. 164 (2016) A54–A60, https://doi.org/10.1149/2.0211702jes.

[19] L. Li, S. Zhao, Z. Hu, S.-.L. Chou, J. Chen, Developing better ester- and ether-based electrolytes for potassium-ion batteries, Chem. Sci. 12 (2021) 2345–2356, https://doi.org/10.1039/D0SC06537D.

[20] R. Verma, P.N. Didwal, J.-.Y. Hwang, C.-.J. Park, Recent progress in electrolyte development and design strategies for next-generation potassium-ion batteries, Batter. Supercaps 4 (2021) 1428–1450, https://doi.org/10.1002/batt.202100029.

[21] Y. Lei, L. Qin, R. Liu, K.C. Lau, Y. Wu, D. Zhai, B. Li, F. Kang, Exploring stability of nonaqueous electrolytes for potassium-ion batteries, ACS Appl. Energy Mater. 1 (2018) 1828–1833, https://doi.org/10.1021/acsaem.8b00214.

[22] S. Liu, L.C. Meyer, L. Medenbach, A. Balducci, Glyoxal-based electrolytes for potassium-ion batteries, Energy Storage Mater. 47 (2022) 534–541, https://doi.org/10.1016/j.ensm.2022.02.041.

[23] L. Ni, G. Xu, C. Li, G. Cui, Electrolyte formulation strategies for potassium-based batteries, Exploration 2 (2022), 20210239, https://doi.org/10.1002/EXP.20210239.

[24] H. Wang, M. Yoshio, KPF_6 dissolved in propylene carbonate as an electrolyte for activated carbon/graphite capacitors, J. Power Sources 195 (2010) 1263–1265, https://doi.org/10.1016/j.jpowsour.2009.08.073.

[25] S. Liu, J. Mao, L. Zhang, W.K. Pang, A. Du, Z. Guo, Manipulating the solvation structure of nonflammable electrolyte and interface to enable unprecedented stability of graphite anodes beyond 2 years for safe potassium-ion batteries, Adv. Mater. 33 (2021), 2006313, https://doi.org/10.1002/adma.202006313.

[26] S. Liu, J. Mao, Q. Zhang, Z. Wang, W.K. Pang, L. Zhang, A. Du, V. Sencadas, W. Zhang, Z. Guo, An intrinsically non-flammable electrolyte for high-performance potassium batteries, Angew. Chem. Int. Ed. 59 (2020) 3638–3644, https://doi.org/10.1002/anie.201913174.

[27] X. Cheng, J. Pan, Y. Zhao, M. Liao, H. Peng, Gel polymer electrolytes for electrochemical energy storage, Adv. Energy Mater. 8 (2018), 1702184, https://doi.org/10.1002/aenm.201702184.

[28] B. Babu, M. Enke, S. Prykhodska, A. Lex-Balducci, U.S. Schubert, A. Balducci, New diglyme-based gel polymer electrolytes for Na-based energy storage devices, ChemSusChem 14 (2021) 4836–4845, https://doi.org/10.1002/cssc.202101445.

[29] M. Armand, Polymer solid electrolytes - an overview, Solid State Ion 9-10 (1983) 745–754, https://doi.org/10.1016/0167-2738(83)90083-8.

[30] H. Gao, L. Xue, S. Xin, J.B. Goodenough, A high-energy-density potassium battery with a polymer-gel electrolyte and a polyaniline cathode, Angew. Chem. Int. Ed. 57 (2018) 5449–5453, https://doi.org/10.1002/anie.201802248.

[31] J. Zheng, L. Schkeryantz, G. Gourdin, L. Qin, Y. Wu, Single potassium-ion conducting polymer electrolytes: preparation, ionic conductivities, and electrochemical stability, ACS Appl. Energy Mater. 4 (2021) 4156–4164, https://doi.org/10.1021/acsaem.1c00483.

[32] M. Rayung, Min.M. Aung, A. Ahmad, Mohd.S. Su'ait, L.C. Abdullah, S.N. Ain Md Jamil, Characteristics of ionically conducting jatropha oil-based polyurethane acrylate gel electrolyte doped with potassium iodide, Mater. Chem. Phys. 222 (2019) 110–117, https://doi.org/10.1016/j.matchemphys.2018.10.009.

[33] N.K. Jyothi, K.K. Venkataratnam, P.N. Murty, K.V. Kumar, Preparation and characterization of PAN–KI complexed gel polymer electrolytes for solid-state battery applications, Bull. Mater. Sci. 39 (2016) 1047–1055, https://doi.org/10.1007/s12034-016-1241-8.

[34] Y. Zhang, A. Bahi, F. Ko, J. Liu, Polyacrylonitrile-reinforced composite gel polymer electrolytes for stable potassium metal anodes, Small 18 (2022), 2107186, https://doi.org/10.1002/smll.202107186.

[35] J. Lang, J. Li, X. Ou, F. Zhang, K. Shin, Y. Tang, A flexible potassium-ion hybrid capacitor with superior rate performance and long cycling life, ACS Appl. Mater. Interfaces 12 (2020) 2424–2431, https://doi.org/10.1021/acsami.9b17635.

[36] K. Lei, F. Li, C. Mu, J. Wang, Q. Zhao, C. Chen, J. Chen, High K-storage performance based on the synergy of dipotassium terephthalate and ether-based electrolytes, Energy Environ. Sci. 10 (2017) 552–557, https://doi.org/10.1039/C6EE03185D.

[37] K. Moyer, J. Donohue, N. Ramanna, A.P. Cohn, N. Muralidharan, J. Eaves, C.L. Pint, High-rate potassium ion and sodium ion batteries by co-intercalation anodes and open framework cathodes, Nanoscale 10 (2018) 13335–13342, https://doi.org/10.1039/C8NR01685B.

[38] N.S. Katorova, S.S. Fedotov, D.P. Rupasov, N.D. Luchinin, B. Delattre, Y.-.M. Chiang, A.M. Abakumov, K.J. Stevenson, Effect of concentrated diglyme-based electrolytes on the electrochemical performance of potassium-ion batteries, ACS Appl. Energy Mater. 2 (2019) 6051–6059, https://doi.org/10.1021/acsaem.9b01173.

[39] X. Liu, G.A. Elia, B. Qin, H. Zhang, P. Ruschhaupt, S. Fang, A. Varzi, S. Passerini, High-power Na-ion and K-ion hybrid capacitors exploiting cointercalation in graphite negative electrodes, ACS Energy Lett. 4 (2019) 2675–2682, https://doi.org/10.1021/acsenergylett.9b01675.

[40] B. Babu, C. Neumann, M. Enke, A. Lex-Balducci, A. Turchanin, U.S. Schubert, A. Balducci, Aging processes in high voltage lithium-ion capacitors containing liquid and gel-polymer electrolytes, J. Power Sources 496 (2021) 229797, https://doi.org/10.1016/j.jpowsour.2021.229797.

[41] P. Isken, M. Winter, S. Passerini, A. Lex-Balducci, Methacrylate based gel polymer electrolyte for lithium-ion batteries, J. Power Sources 225 (2013) 157–162, https://doi.org/10.1016/j.jpowsour.2012.09.098.

[42] B. Babu, A. Balducci, Self-discharge of lithium-ion capacitors, J. Power Sources Adv. 5 (2020), 100026, https://doi.org/10.1016/j.powera.2020.100026.

[43] T. Palaniselvam, B. Babu, H. Moon, I. Hasa, A.L. Santhosha, M. Goktas, Y.-.N. Sun, L. Zhao, B.-.H. Han, S. Passerini, A. Balducci, P. Adelhelm, Tin-containing graphite for sodium-ion batteries and hybrid capacitors, Batter. Supercaps 4 (2021) 173–182, https://doi.org/10.1002/batt.202000196.

[44] S.P. Varghese, B. Babu, V. Surendran, D. Damien, R. Antony, M.M. Shaijumon, γ-MnOOH-graphene nanocomposite as promising anode material for Li-ion capacitors, J. Energy Storage 47 (2022), 103636, https://doi.org/10.1016/j.est.2021.103636.

[45] B. Babu, S.G. Ullattil, R. Prasannachandran, J. Kavil, P. Periyat, M.M. Shaijumon, Ti3+ induced brown TiO2 nanotubes for high performance sodium-ion hybrid capacitors, ACS Sustain. Chem. Eng. 6 (2018) 5401–5412, https://doi.org/10.1021/acssuschemeng.8b00236.

[46] V. Surendran, R.S. Arya, T.V. Vineesh, B. Babu, M.M. Shaijumon, Engineered carbon electrodes for high performance capacitive and hybrid energy storage, J. Energy Storage 35 (2021), 102340, https://doi.org/10.1016/j.est.2021.102340.

[47] S.T. Oswald, F. Zier, M. Hoffmann, M. Jaumann, T. Herklotz, M. Nikolowski, K. Scheiba, F. Kohl, M. Giebeler, L. Mikhailova, D. Ehrenberg, H., Binding energy referencing for XPS in alkali metal-based battery materials research (II): application to complex composite electrodes, Batteries 4 (2018) 36, https://doi.org/10.3390/batteries4030036.

[48] X. Zhang, Y. Yang, X. Qu, Z. Wei, G. Sun, K. Zheng, H. Yu, F. Du, Layered P2-type K0.44Ni0.22Mn0.78O2 as a high-performance cathode for potassium-ion batteries, Adv. Funct. Mater. 29 (2019), 1905679, https://doi.org/10.1002/adfm.201905679.

[49] Y. Han, A.P. Vijaya Kumar Saroja, H.R. Tinker, Y. Xu, Interphases in the electrodes of potassium ion batteries, J. Phys.: Mater. 5 (2022), 022001, https://doi.org/10.1088/2515-7639/ac5dce.